Journal of Alloys and Compounds 626 (2015) 368–374

Contents lists available at ScienceDirect

Journal of Alloys and Compounds

journal homepage: www.elsevier.com/locate/jalcom

Spark plasma sintered bismuth telluride-based thermoelectric materials incorporating dispersed boron carbide

H.R. Williams [a,*], R.M. Ambrosi [b], K. Chen [c], U. Friedman [a,1], H. Ning [c], M.J. Reece [c], M.C. Robbins [d], K. Simpson [d], K. Stephenson [e]

[a] Department of Engineering, University of Leicester, University Road, Leicester LE1 7RH, UK
[b] Space Research Centre, Department of Physics and Astronomy, University of Leicester, University Road, Leicester LE1 7RH, UK
[c] School of Engineering & Materials Science, Queen Mary, University of London, Mile End Road, London E1 4NS, UK
[d] European Thermodynamics Ltd., 8 Priory Business Park, Wistow Road, Kibworth LE8 0R, UK
[e] European Space Agency, ESTEC TEC-EP, Keplerlaan 1, 2201AZ Noordwijk, The Netherlands

ARTICLE INFO

Article history:
Received 12 August 2014
Received in revised form 25 November 2014
Accepted 3 December 2014
Available online 13 December 2014

Keywords:
Thermoelectric materials
Sintering
Mechanical properties

ABSTRACT

The mechanical properties of bismuth telluride based thermoelectric materials have received much less attention in the literature than their thermoelectric properties. Polycrystalline p-type $Bi_{0.5}Sb_{1.5}Te_3$ materials were produced from powder using spark plasma sintering (SPS). The effects of nano-B_4C addition on the thermoelectric performance, Vickers hardness and fracture toughness were measured. Addition of 0.2 vol% B_4C was found to have little effect on zT but increased hardness by approximately 27% when compared to polycrystalline material without B_4C. The K_{IC} fracture toughness of these compositions was measured as 0.80 MPa $m^{1/2}$ by Single-Edge V-Notched Beam (SEVNB). The machinability of polycrystalline materials produced by SPS was significantly better than commercially available directionally solidified materials because the latter is limited by cleavage along the crystallographic plane parallel to the direction of solidification.

1. Introduction

Improving the mechanical properties of thermoelectric materials may enable higher reliability and performance in thermoelectric generator systems. Thermoelectric devices have been applied to numerous energy conversion applications, some of the most demanding being in Radioisotope Thermoelectric Generator (RTG) systems for deep space and planetary exploration missions [1–3]. To-date, these power systems use the heat generated from the nuclear decay of plutonium-238, which is then converted into electricity by lead telluride or silicon–germanium thermoelectric materials. Systems under development for potential future application in Europe would use americium-241 due to its lower cost [3]. Am-241 has approximately one quarter of the energy density of Pu-238 [3,4], which will lead to lower temperatures and heat flux through the thermoelectric elements; this drives the selection of bismuth telluride thermoelectric materials with high aspect-ratio (long) legs [5]. A key advantage of bismuth telluride based materials is that proven module manufacturing approaches are available, which lowers technical development risk. However, poor mechanical properties of directionally solidified material mean that modules with high aspect-ratio legs are difficult to manufacture [6] and the capacity to withstand loads in service is a concern. The aim of this paper is to investigate and develop novel bismuth telluride based thermoelectric materials with improved mechanical properties relative to conventional directionally solidified materials.

The highest thermoelectric figure of merit (zT) is achieved in materials produced in directionally solidified form, *parallel* to the direction of solidification [7]. The strength and toughness is poor *perpendicular* to solidification due to cleavage along the basal crystallographic plane which is aligned parallel to the growth direction [7–9]. Strength is also governed by flaws [10] in common with any brittle solid. Mechanical property improvement has been the justification for the development of polycrystalline materials produced by a variety of processes including hot-pressing [11,12], extrusion [8,13], plasma activated sintering [14,15] and spark plasma sintering (SPS) [7,16–24]. The addition of nanoscale particulate reinforcements (SiC [17,18,23], C_{60} [7], multi-wall carbon nanotubes [12] and Al_2O_3 [22]) have been pursued. The intention is to maintain thermoelectric performance in polycrystalline materials while improving their mechanical properties.

Key results and trends from the literature are summarised in Table 1, which has been arranged to highlight comparative results

* Corresponding author. Tel.: +44 (0)116 223 1052.
E-mail address: hugo.williams@leicester.ac.uk (H.R. Williams).
[1] Now at Illston & Robson Ltd., Birmingham, UK.

http://dx.doi.org/10.1016/j.jallcom.2014.12.010
0925-8388/

Table 1
Summary of reported properties.[a]

	Directionally solidified materials (Bridgman/Zone melting)	Polycrystalline materials	Polycrystalline–dispersed particle composite
Hardness ($kgf\,mm^{-2}$)	53 HV0.01 (⊥) 48 HV0.01 (‖) [14]	113 HV0.01 100 HV0.025 [14] 56–65 HV [8] 45–64 HV [19] 55–57 HV [24] 63 HV0.5 [18] 83 HV1 [23]	 74–80 HV0.5 [18] 87 HV1 [23]
Flexural strength[b] (MPa)	45 (⊥) 80 (‖) [10] 35 (⊥) 50 (‖) [10] (Equibiaxial) 9.6 (⊥), 54(‖) [9] 20 [11]	50 [11] 40, 61 [13] 73 [16] 32 [12] (Equibiaxial) 66 [23]	 90 [12] (Equibiaxial) 74 [23]
Indentation fracture Toughness ($MPa\,m^{1/2}$)		1.14 [18] 0.82 [23]	1.19–1.35 [18] 0.91 [23]
zT[c]	Best room temperature values of up to 1.3 quoted [14]. More typically 1.1 (‖) and 0.8 (⊥) [7,9]	Best room temperature values of up to 1.1 (⊥) and 0.8 (‖) quoted [7], typical value 0.9 (⊥) [16,19]. Note: max zT occurs ⊥, the opposite of directionally solidified material	Increased relative to respective controls for: 0.1 vol% SIC to zT = 1.0 [18] (n-type) 0.5 vol% Al_2O_3 to zT = 1.2 [22]

[a] ⊥ is perpendicular to direction of solidification or pressing, ‖ is parallel; see Fig. 1.
[b] 3 point bending except where indicated.
[c] p-type values quoted except where indicated, n-type values typically lower.

from the same study. Material orientations used for Vickers indentation and flexural strength are illustrated schematically in Fig. 1. A wide range of different process variables and test methods have been considered which makes direct comparisons difficult. However, by comparing results within the same study there is a pattern of improving hardness, strength and toughness when moving from directionally solidified to polycrystalline materials and then to composite material forms. In contrast, moving from directionally solidified to polycrystalline materials generally reduces zT. In pressed or sintered materials the direction of maximum zT switches from *parallel* with solidification to *perpendicular* to the pressing direction. This effect has been attributed to preferential alignment of the basal poles with the pressing direction [7]. The addition of a dispersed nanoscale particle phase may increase the zT relative to a control polycrystalline specimen providing the volume fraction is optimised, largely due to reduced thermal conductivity [18,22,23].

The objective of this work was to perform a characterisation of p-type bismuth telluride based thermoelectric $Bi_{0.5}Sb_{1.5}Te_3$ with dispersed nano-scale boron carbide (B_4C). Vickers hardness, fracture toughness and thermoelectric properties were measured. The p-type material was selected for this study based on experience of commercial module manufacture, where the mechanical properties of commercial p-type material have proved more limiting than commercial n-type materials. The high hardness of B_4C is expected to enhance the mechanical properties. Mechanical tests have also been performed on a commercially available directionally solidified material. The indentation size effect [25] and anisotropy in hardness measurements are investigated. The single-edge V-notched beam (SEVNB) fracture toughness test method was selected in preference to the indentation fracture toughness method, since the latter has been found to be unreliable [26].

2. Experimental

2.1. Material preparation

Materials were manufactured by mechanical alloying and spark plasma sintering from commercially available Bi (Aldrich 99.5%, 100 mesh), Sb (Aldrich 99.5%, 100 mesh), Te (Alfa Aesar 99.999%, 18–60 mesh) and B_4C (H.C. Starck, 96.3%, 300 nm). The basic thermoelectric composition was $Bi_{0.5}Sb_{1.5}Te_3$ and nanoparticle dispersion was investigated at volume fractions of 0, 0.1, 0.2 and 0.5 vol% B_4C. These fractions were selected based on previous work using SiC and Al_2O_3 [17,18,22,23] to allow comparison. The powders were ball milled in stainless steel pots with stainless steel balls at 350 rpm for 10 h in a planetary ball mill (QM-3SP2, Nanjing University Instrument Plant, China). The mill direction was paused for 5 min every hour and the direction of milling reversed. No milling medium was used and a 10:1 ball

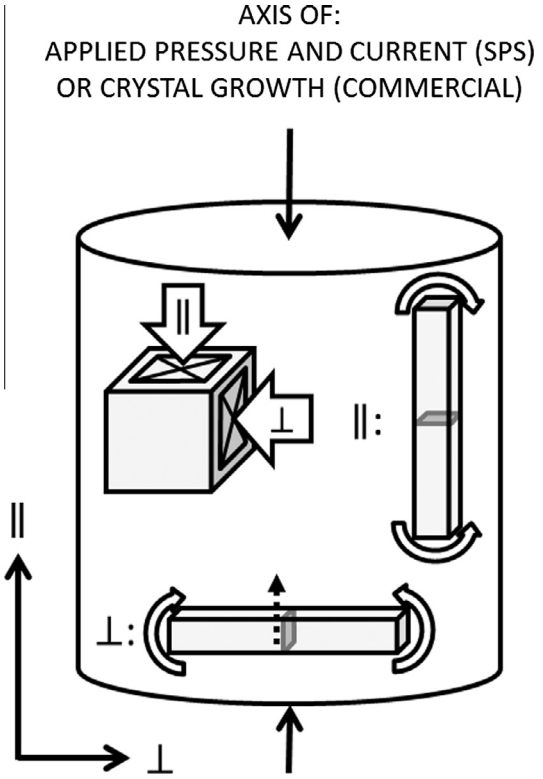

Fig. 1. Material property orientation for indentation and flexure. Fracture plane is shown shaded. Dotted arrow on perpendicular flexural specimen indicates direction of crack growth for SEVNB tests reported in this study. No distinction is made between radial and circumferential components of the perpendicular direction.

to powder ratio selected. The powders were then sintered in a spark plasma sintering furnace (HPD 25/1; FCT, Rauenstein, Germany) at 450 °C and 57 MPa for 5 min. A density greater than 99% of theoretical density was achieved for all compositions. Commercial n- and p-type thermoelectric materials (Everredtronics, China) produced by directional solidification were obtained for comparison.

2.2. Test methodology

The microstructures of the samples were observed using a Scanning Electron Microscope (FEI, Inspect F). Seebeck coefficient and electrical resistivity were measured perpendicular to the direction of applied pressure by a Namicro-II measurement system (China). The thermal conductivity was obtained from the product of thermal diffusivity, specific heat and density. The thermal diffusivity was measured using the laser flash method (NETZSCH, LFA457, Germany) in the direction parallel to the applied pressure. The density of the samples was measured using the Archimedes method. The specific heat was determined using differential scanning calorimetry (NETZSCH, DSC 404C, Germany). Vickers Hardness testing was performed using a micro hardness tester (SHIMADZU, Japan) at applied loads of 0.05, 0.1, 0.2, 0.5 and 1 kg. Five indentations were performed in the direction of applied pressure (parallel, ∥) at each load and a mean taken. Following initial results some specimen types were also tested in the perpendicular (⊥) orientation with single indentations at each failure load. Fracture toughness testing by single-edge V-notch beam (SEVNB) [27] was performed in an articulated four-point bending fixture with a support span of 20.25 mm and load span of 7.75 mm using beam specimens of dimensions 3 × 4 × 25 mm. This is a narrow span configuration option for which corrections to the fracture toughness expressions were applied; the fracture toughness was calculated using [27,28]:

$$K_{IC} = \frac{F_c}{B\sqrt{W}} \frac{S_1 - S_2}{W} \frac{3\sqrt{a}}{2(1-\alpha)^{1.5}} Y \quad (1)$$

$$\text{where}: Y = 1.1215\sqrt{\pi}\left[\frac{5}{8} - \frac{5}{12}\alpha + \frac{1}{8}\alpha^2 + 5\alpha^2(1-\alpha)^6 + \frac{3}{8}\exp\left(-6.1342\frac{\alpha}{1-\alpha}\right)\right] \quad (2)$$

In these relations, F_c is the failure load, S_1 and S_2 are the spans of bottom and top support rollers respectively, W and B are the height and width of the specimen respectively and α is the ratio of crack length (a) to specimen height (W). Specimens were machined using a diamond saw with the final V-notch being ground by hand using a razor blade and 6 μm diamond paste. All specimens were oriented such that the fracture toughness was measured with bending stress applied in the direction perpendicular to the sintering pressure or crystal growth, and the crack plane and crack growth direction parallel, as illustrated by the perpendicular beam specimen in Fig. 1. This orientation maximised the number of tests specimens available from a given amount of material and represents the bounding case of poor toughness in directionally solidified material. The V-notch depth was periodically checked during grinding, and finally measured after failure in three locations using an Olympus SZX12 optical microscope. This microscope was also used to inspect the fracture surfaces. Testing was performed using an Instron 3343 test frame with $a \pm 500$ N load cell operated in displacement control at 0.5 mm min^{-1} at ambient temperature and pressure.

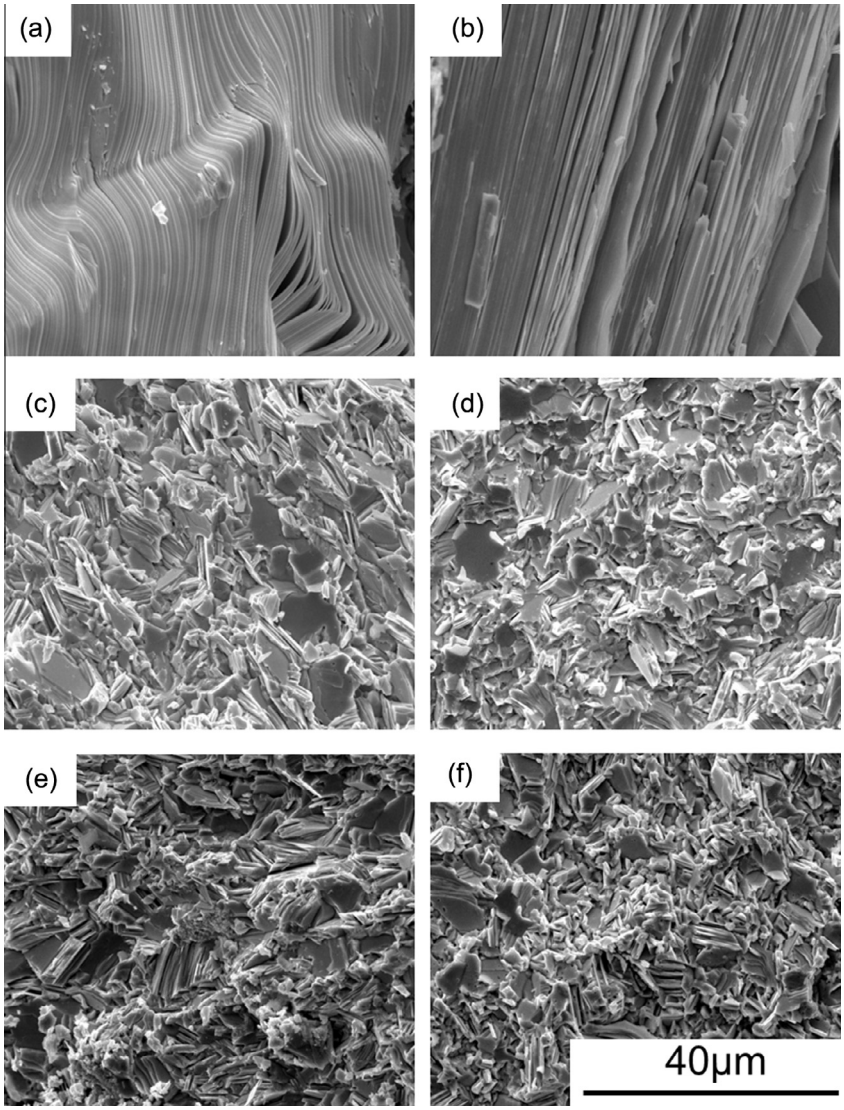

Fig. 2. SEM fractographs of bismuth telluride based materials: (a) Commercial directionally solidified n-type Bi_2Te_3; (b) commercial directionally solidified p-type $Bi_{0.5}Sb_{1.5}Te_3$; (c) p-type $Bi_{0.5}Sb_{1.5}Te_3$ produce by mechanical alloying and SPS; (d) $Bi_{0.5}Sb_{1.5}Te_3$ + 0.1vol% B_4C; (e) $Bi_{0.5}Sb_{1.5}Te_3$ + 0.2vol% B_4C; and (f) $Bi_{0.5}Sb_{1.5}Te_3$ + 0.5vol% B_4C.

3. Results and discussion

3.1. Microstructure

Scanning Electron Microscopy (SEM) images of the fractured surfaces of the materials are shown in Fig. 2. The characteristic directional, lamellar microstructure is evident in the commercial n- and p-type materials. Specimens produced by SPS show an approximately equiaxed microstructure with an evident reduction in grain size as the volume fraction of B_4C is increased. The grains sizes were estimated manually from these images as ~3 μm with no B_4C, reducing to ~2 μm with 0.5 vol% B_4C. Fig. 3 shows the B_4C particles are mostly concentrated at the grain boundaries, supporting the argument that they suppress grain growth. The results are consistent with previously reported work using nano-SiC dispersion [23].

3.2. Thermoelectric properties

The measured thermoelectric properties are shown in Figs. 4 and 5. The trends are broadly in agreement with the literature on p-type bismuth telluride based materials produced using SPS and reinforced with nano-scale phases [7,12,14,16,20–23]. The data in Fig. 4 show generally lower Seebeck coefficient and electrical resistivity than some of the reports in the literature, but the overall performance, indicated by the zT values in Fig. 5, are similar. In this work, to allow efficient usage of material and consistent process settings, the Seebeck and resistivity values are measured in the direction perpendicular to the sintering pressure, while the thermal conductivity is measured in the direction parallel to the applied pressure. The Seebeck and resistivity data are presented in Fig. 4 with the resulting power factor, showing that 0.1 and 0.2 vol% B_4C have little deleterious effect on performance for a fixed temperature difference, but addition of 0.5 vol% B_4C does start to reduce potential power output. Power factor is a sound means of assessing potential power output for a fixed temperature across a thermoelectric, but in RTG applications the temperature difference is not fixed because the system is power-limited [5], so some estimate of zT is better means to evaluate the effect on system performance. Fig. 5 shows the thermal conductivity and a comparative zT calculated using the data in Figs. 4 and 5(a). This is a 'hybrid' zT value appropriate for a comparative study of the effect of B_4C addition, but requires care when comparing to the literature because thermoelectric properties may be anisotropic, even in polycrystalline materials. Several literature reports do

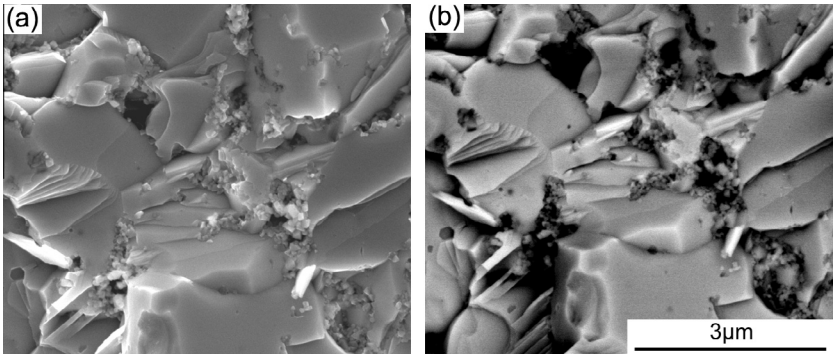

Fig. 3. High-resolution SEM images using (a) secondary and (b) backscatter electron of $Bi_{0.5}Sb_{1.5}Te_3$ + 0.5 vol% B_4C with nano-B_4C particles concentrated at the grain boundaries.

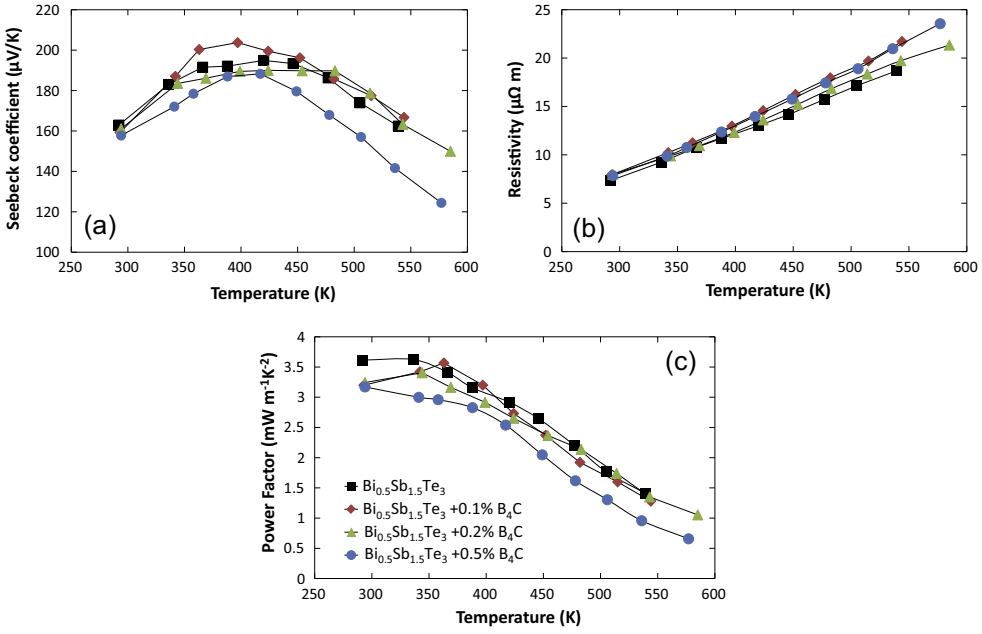

Fig. 4. Effect of B_4C addition on power factor (⊥) of $Bi_{0.5}Sb_{1.5}Te_3$ produced by SPS.

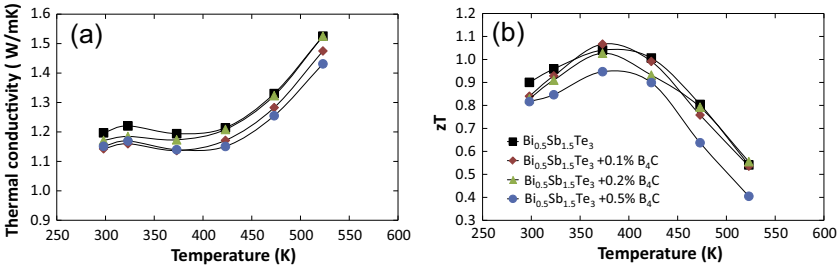

Fig. 5. (a) Thermal conductivity (||) and (b) a comparative zT suitable for estimating the thermoelectric performance variation with volume fraction of B_4C for the given processing conditions.

not clearly state the direction in which the thermoelectric properties are measured; which further complicates any comparison. For similar materials to those studied herein, thermal conductivity may be lower in the direction parallel to pressing, but this depends on powder morphology and processing [21]. If this trend did apply to the data in Fig. 5, then the presented zT would be a slight overestimate of the performance perpendicular to the direction of applied pressure.

The addition of B_4C has a small effect on the electrical resistivity, reduces Seebeck coefficient and reduces thermal conductivity. The comparative zT performance remains little changed for additions of 0.1 vol% and 0.2 vol% B_4C because the slight reduction in power factor is offset by reduced thermal conductivity, but is significantly reduced as the nanoparticle fraction reaches 0.5 vol% B_4C. Based on these data, $Bi_{0.5}Sb_{1.5}Te_3$ + 0.2 vol% B_4C was selected for a more detailed mechanical characterisation as it was expected to offer improved mechanical performance with minimal effect on thermoelectric performance. There may be scope to optimise the processing parameters to improve thermoelectric properties in future work.

3.3. Vickers hardness

The Vickers hardness for all of the compositions, measured parallel to the direction of applied pressure during SPS processing or crystal growth (commercial materials) is given in Fig. 6. The data are consistent with the results from the literature summarised in Table 1, and show an improvement in hardness resulting from the addition of B_4C. This corresponds with the grain size reduction shown in Fig. 2. Fig. 6(a) also shows, with the exception of an occasional anomalous data point, the characteristic indentation size effect in brittle materials; reducing hardness with increasing indentation load tending to a limit [25]. Taking the value at the highest indentation load of 1 kgf to minimise the influence of indentation sizes, the addition of 0.2 vol% B_4C to the material produced by SPS increases the hardness by 27%. Across the range of indentation loads and directions measured, the increase in hardness varies from 6% to 34%. The anisotropy of mechanical properties is characterised in Fig. 6(b), showing significantly higher hardness perpendicular to the direction of applied pressure during SPS. For the polycrystalline materials produced by SPS, the hardness increases by 50% in the perpendicular direction compared to the parallel direction. The directionally solidified commercial n-type material is also notably harder in the direction perpendicular to solidification, while there is little difference for the p-type. This result quantifies the observation that the p-type commercial material is a more difficult material to machine and assemble into modules. Perpendicular indentations for both the n- and p-type generated parallel cracks along the weakly bonded cleavage plane; this is illustrated for the n-type material in Fig. 7 in comparison to the SPS-produced material containing B_4C. The increased perpendicular direction hardness measured in the n-type material occurs in spite of this failure mechanism and highlights one limitation of using hardness as an indication of strength in this group of materials.

Nanoparticle reinforcement by B_4C, even at a low volume fraction of 0.2 vol%, yields a significant improvement in the hardness of the material over and above the benefit of a polycrystalline microstructure. The direction of higher hardness coincides with the direction of higher thermoelectric performance described in the literature.

3.4. Fracture toughness

Fracture toughness was measured using the SEVNB method for four specimen groups, selected based upon the results of the thermoelectric property testing. The standard commercial n- and p-type materials were prepared as controls to be compared with

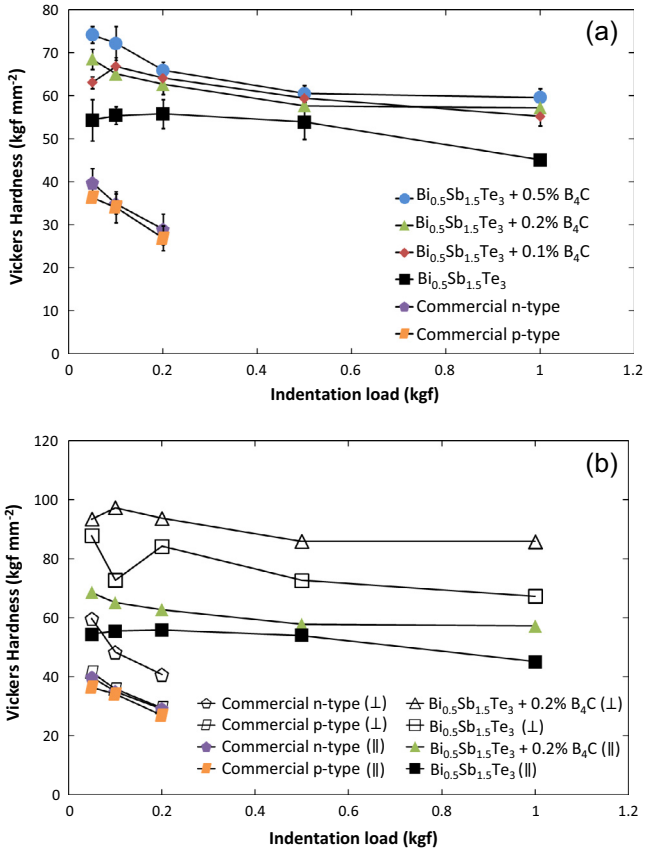

Fig. 6. Hardness of bismuth telluride materials: (a) in the direction parallel (||) to applied pressure or crystal growth; and (b) in comparison with perpendicular (⊥) direction for selected compositions.

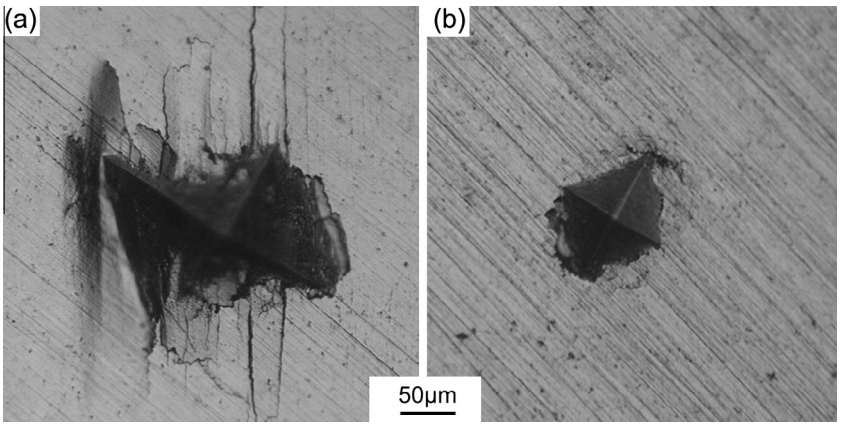

Fig. 7. Comparison of 0.5 kgf Vickers indentations performed in the perpendicular direction on: (a) n-type directionally solidified material and (b) $Bi_{0.5}Sb_{1.5}Te_3$ + 0.2% B_4C produced by SPS.

Table 2
Fracture toughness (SEVNB) results.

Specimen	No. valid failures/ no. specimens tested	Fracture toughness K_{Ic} (MPa $m^{1/2}$) ±1σ
Commercial n-type, directionally solidified	1[a]/6	Single valid data-point only: 0.64
Commercial p-type, directionally solidified	1[a]/6	Single valid data-point only: 0.60
$Bi_{0.5}Sb_{1.5}Te_3$: SPS	5/5	0.79 ± 0.03
$Bi_{0.5}Sb_{1.5}Te_3$ + 0.2 vol% B_4C: SPS	6/6	0.80 ± 0.01

[a] Invalid failures were re-evaluated as 4 point-bend flexural specimens as discussed in text.

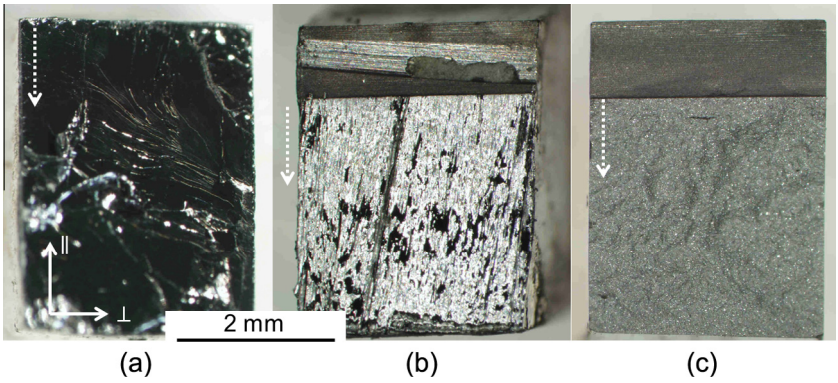

Fig. 8. Fracture surfaces of fracture toughness specimens (⊥): (a) of a directionally solidified p-type specimen that failed remote from the V-notch; (b) a directionally solidified p-type specimen that failed from the V-notch; (c) $Bi_{0.5}Sb_{1.5}Te_3$ SPS specimen failing on the V-notch. Dotted arrow shows direction of crack growth.

the SPS produced $Bi_{0.5}Sb_{1.5}Te_3$ without B_4C, and with 0.2 vol% B_4C. The results are summarised in Table 2.

The directionally solidified materials proved to have insufficient toughness to register valid failure modes, with all but one of each specimen group failing remote from the V-notch at very low loads. A typical fracture surface of a specimen that failed remote from the V-notch is shown in Fig. 8(a), and is consistent with previously reported failure on the cleavage plane [9]. Fig. 8(b) shows the fracture surface of one of the directionally solidified specimens that failed at the V-notch, showing more conventional brittle fracture. The polycrystalline nature of the material produced by SPS is readily apparent in Fig. 8(c). The flexural strength of the directionally solidified specimens that failed remote from the V-notch was calculated assuming a conventional four-point bending configuration. For both the n- and p-type specimens the mean flexural strength was less than 4 MPa, with no statistically significant difference between the groups. Although this value is lower than the ~9 MPa reported by Zheng et al. [9], it is of the same order of magnitude and provides some confidence that the material behaviour is representative.

In contrast the specimens produced by SPS generated a very narrow range of similar fracture toughness values. A Student's t-test confirms that the difference between the fracture toughness values for the two SPS specimen groups is not significant based on these data.

It has not been possible to quantify the fracture toughness improvement in a bismuth telluride based thermoelectric material produced by SPS over directional solidification because the fracture toughness of the latter is too low to achieve valid failures using this test. It is possible to conclude qualitatively that manufacture by SPS offers an improvement in fracture toughness over conventional directional solidification. Further qualitative evidence is provided by the observation that the SPS test specimens are much more easily machined, with much less tendency to split and fracture. This is, in itself, a key benefit of this material for thermoelectric module production.

The fracture toughness values measured for these materials are lower than previously reported values summarised in Table 1. However, these previous values were obtained using the indentation fracture toughness technique and are not directly comparable. A direct comparative study on skutterudite thermoelectric materials highlights the benefits of the SEVNB approach [26]. The present study is, to the best of the authors' knowledge, the first published report of SEVNB fracture toughness results for bismuth telluride based materials.

4. Concluding remarks and future work

Polycrystalline $Bi_{0.5}Sb_{1.5}Te_3$ (p-type) materials reinforced with up to 0.5 vol% B_4C were produced from powders by mechanical alloying and spark plasma sintering. The thermoelectric properties of the materials produced were consistent with literature reports for other nanoparticle reinforcements. Addition of up to 0.2 vol% B_4C had little deleterious effect on zT. The addition of 0.2 vol% B_4C improved the Vickers hardness by approximately 27% compared to SPS material alone and, for these two materials, hardness was found to be 50% higher when measured perpendicular to the direction of applied sintering pressure compared to parallel. The K_{IC} fracture toughness of polycrystalline $Bi_{0.5}Sb_{1.5}Te_3$ materials reinforced with up 0.2 vol% B_4C was measured by single-edge V-notched beam (SEVNB) as 0.80 MPa $m^{1/2}$, with no statistically significant difference achieved with the addition of B_4C at this low volume fraction. Sufficient valid failures could not be obtained using this test for directionally solidified commercial material due to cleavage along weak crystallographic planes causing failure remote from the V-notch. Whilst the invalid failure precludes a *quantitative* comparison, it is a clear *qualitative* indication of the serious lack of fracture toughness in the directionally solidified materials.

These material data suggest significant scope for improving the mechanical properties of thermoelectric modules used in applications such as Radioisotope Power Systems for spacecraft. Further evaluation of B_4C, including optimisation of the processing conditions and volume fractions is supported by the preliminary results presented herein. Wider standardisation of the appropriate methodologies for mechanical characterisation of thermoelectric materials is highly desirable to allow robust comparison between different studies, mechanical design and failure investigation of thermoelectric modules.

Acknowledgements

This work was performed under contract to the European Space Agency under the Thermoelectric Converter for Small-Scale RTG programme, 23026/10/NL/AT. The authors wish to express their thanks to the reviewers for their suggested improvements to the manuscript.

References

[1] R.G. Lange, W.P. Caroll, Review of recent advances of radioisotope power systems, Energy Convers. Manage. 49 (2008) 393–401, http://dx.doi.org/10.1016/j.enconman.2007.10.028.
[2] G.H. Fountain, D.Y. Kusnierkiewicz, C.B. Hersman, T.S. Herder, T.B. Coughlin, et al., The New Horizons spacecraft, Space Sci. Rev. 140 (2008) 23–47, http://dx.doi.org/10.1007/s11214-008-9374-8.
[3] L. Summerer, K. Stephenson, Nuclear power sources: a key enabling technology for planetary exploration, proceedings IMechE G, Aerospace Eng. 225 (2011) 129–142, http://dx.doi.org/10.1243/09544100JAERO766.
[4] H.R. Williams, H. Ning, M.J. Reece, R.M. Ambrosi, et al., Metal matrix composite fuel for space radioisotope energy sources, J. Nucl. Mater. 433 (2013) 116–123. doi:10.1016/j.jnucmat.2012.09.030.
[5] H.R. Williams, R.M. Ambrosi, N.P. Bannister, et al., A conceptual spacecraft radioisotope thermoelectric and heating unit (RTHU), Int. J. Energy Res. 36 (2012) 1192–1200, http://dx.doi.org/10.1002/er.1864.
[6] D.E. Wesolowski, R.S. Goeke, A.M. Morales, S.H. Goods, P.A. Sharma, et al., Development of a Bi_2Te_3-based thermoelectric generator with high-aspect ratio free-standing legs, J. Mater. Res. 27 (2012) 1149–1156, http://dx.doi.org/10.1557/jmr.2012.27.
[7] N. Gothard, G. Wilks, T.M. Tritt, J.E. Spowart, Effect of processing route on the microstructure of thermoelectric properties of bismuth telluride based alloys, J. Electron. Mater. 39 (2010) 1909–1913, http://dx.doi.org/10.1007/s11664-009-1051-5.
[8] S.J. Hong, B.S. Chun, Microstructure and thermoelectric properties of extruded n-type 95%Bi_2Te_2–5%Bi_2Se_3 alloy along bar length, Mater. Sci. Eng. A 356 (2003) 345–351, http://dx.doi.org/10.1016/S0921-5093(03)00147-3.
[9] Y. Zheng, H. Xie, S. Shu, Y. Yan, H. Li, X. Tang, High-temperature mechanical and thermoelectric properties of p-type $Bi_{0.5}Sb_{1.5}Te_3$ commercial zone melting ingots, J. Electron. mater. 43 (2014) 2017–2022, http://dx.doi.org/10.1007/s11664-013-2938-8.
[10] A.A. Wereszczak, T.P. Kirkland, O.M. Jadaan, H. Wang, Strength of bismuth telluride, in: S. Priya, A. Weidenkaff, D.P. Norton, D. Singh, J. Salem (Eds.), Advances in Electronic Ceramics II, John Wiley & Sons, Inc., Hoboken, NJ, USA, 2010. doi: 10.1002/9780470584422.ch11.
[11] H.S. Shin, H.P. Ha, D.B. Hyun, J.D. Shim, D.H. Lee, Thermoelectric properties of 25%Bi_2Te_3–75%Sb_2Te_3 solid solution prepared by hot-pressing method, J. Phys. Chem. Solids 58 (1997) 671–678, http://dx.doi.org/10.1016/S0022-3697(96)00049-2.
[12] F. Ren, H. Wang, P.A. Menchhofer, J.O. Kiggans, Thermoelectric and mechanical properties of multi-walled carbon nanotube doped $Bi_{0.4}Sb_{1.6}Te_3$ thermoelectric material, Appl. Phys. Lett. 103 (2013) 221907, http://dx.doi.org/10.1063/1.4834700.
[13] K. Park, J.H. Seo, D.C. Cho, B.H. Choi, C.H. Lee, Thermoelectric properties of p-type Te doped $Bi_{0.5}Sb_{1.5}Te_3$ fabricated by powder extrusion, Mater. Sci. Eng. B 88 (2002) 103–106, http://dx.doi.org/10.1016/S0921-5107(01)00912-6.
[14] X.A. Fan, J.Y. Yang, R.G. Chen, H.S. Yun, W. Zhu, et al., Characterization and thermoelectric properties of p-type 25%Bi_2Te_3–75%Sb_2Te_3prepared via mechanical alloying and plasma activated sintering, J. Phys. D Appl. Phys. 39 (2006) 740–745, http://dx.doi.org/10.1088/0022-3727/39/4/021.
[15] X.A. Fan, J.Y. Yang, W. Zhu, H.S. Yun, R.G. Chen, et al., Microstructure and thermoelectric properties of n-type $Bi_2Te_{2.85}Se_{0.15}$ prepared by mechanical alloying and plasma activated sintering, J. Alloys Comp. 420 (2006) 256–259, http://dx.doi.org/10.1016/j.jallcom.2005.10.025.
[16] D.M. Lee, C.H. Lim, S.Y. Shin, D.C. Cho, C.H. Lee, Thermoelectric properties of p-type Bi0.5Sb1.5Te3 compounds fabricated by spark plasma sintering, J. Electroceram. 17 (2006) 879–883, http://dx.doi.org/10.1007/s10832-006-6807-1.
[17] J.F. Li, J. Liu, Effect of nano-SiC dispersion on thermoelectric properties of Bi_2Te_3polycrystals, Physica Status Solidi A 203 (2006) 3768–3773, http://dx.doi.org/10.1002/pssa.200622011.
[18] L.D. Zhao, B.P. Zhang, J.F. Li, et al., Thermoelectric and mechanical properties of nano-SiC-dispersed Bi_2Te_3 fabricated by mechanical alloying and spark plasma sintering, J. Alloys Comp. 455 (2008) 259–264, http://dx.doi.org/10.1016/j.jallcom.2007.01.015.
[19] C.D. Moon, S. Shin, D.H. Kim, T.S. Kim, Microstructure and thermoelectric properties of p-type Bi_2Te_3–Sb_2Te_3 alloys produced by rapid solidification and spark plasma sintering, J. Alloys Comp. 504S (2010) S504–S507, http://dx.doi.org/10.1016/j.jallcom.2010.03.114.
[20] C.D. Moon, T.S. Kim, The microstructure and thermoelectric properties of rapid solidified p-type Sb_2Te_3-25%Bi_2Te_3 alloys, J. Alloys Comp. 536S (2012) S559–S563, http://dx.doi.org/10.1016/j.jallcom.2012.01.112.
[21] D.H. Kim, C. Kim, S.H. Heo, H. Kim, Influence of powder morphology on thermoelectric anisotropy of spark-plasma-sintered Bi–Te-based thermoelectric materials, Acta Materialia 59 (2011) 405–411, http://dx.doi.org/10.1016/j.actamat.2010.09.054.
[22] K.T. Kim, G.H. Ha, Fabrication and enhanced thermoelectric properties of alumina nano-particle-dispersed $Bi_{0.5}Sb_{1.5}Te_3$ matrix composites, J. nanomater. 2013 (2013) 821657, http://dx.doi.org/10.1155/2013/821657.
[23] D.W. Liu, J.F. Li, C. Chen, B.P. Zhang, Effects of SiC nanodispersion on the thermoelectric properties of p-type and n-type Bi_2Te_3 based alloys, J. Electron. Mater. 40 (2011) 992–998, http://dx.doi.org/10.1007/s11664-010-1476-x.
[24] H.S. Kim, S.J. Hong, Thermoelectric properties of n-type 95%Bi_2Te_2-5%Bi_2Se_3 compounds fabricated by gas-atomization and spark plasma sintering, J. Alloys Comp. 586 (2014) S428–S431, http://dx.doi.org/10.1016/j.jallcom.2013.05.163.
[25] J.B. Quinn, G.D. Quinn, Indentation brittleness of ceramics: a fresh approach, J. Mater. Sci. 32 (1997) 4331–4346, http://dx.doi.org/10.1023/A:1018671823059.
[26] J. Eilertsen, M.A. Subramanian, J.J. Kruzic, Fracture toughness of Co_4Sb_{12} and $In_{0.1}Co_4Sb_{12}$ thermoelectric skutterudites evaluated by three methods, J. Alloys Comp. 552 (2013) 489–492, http://dx.doi.org/10.1016/j.jallcom.2012.11.066.
[27] J. Kübler, Fracture toughness of ceramics using the SEVNB method: round robin, VMAS report No. 37. (1999), ESIS Document D2–99.Dübendorf, Switzerland, EMPA.
[28] T. Fett, D. Munz, Stress intensity factors and weight functions, Computational Mechanics Publications, Southampton, UK, 1997. P. 107.